Microporous and Mesoporous Materials 146 (2011) 36–47

Contents lists available at ScienceDirect

Microporous and Mesoporous Materials

journal homepage: www.elsevier.com/locate/micromeso

A co-templating route to the synthesis of Cu SAPO STA-7, giving an active catalyst for the selective catalytic reduction of NO

A. Lorena Picone [a], Stewart J. Warrender [a], Alexandra M.Z. Slawin [a], Daniel M. Dawson [a], Sharon E. Ashbrook [a], Paul A. Wright [a,*], Stephen P. Thompson [b], Lucia Gaberova [c], Philip L. Llewellyn [c], Beatrice Moulin [d], Alexandre Vimont [d], Marco Daturi [d], Min Bum Park [e], Sam Kyung Sung [e], In-Sik Nam [e], Suk Bong Hong [e]

[a] EASTCHEM School of Chemistry, University of St. Andrews, Purdie Building, North Haugh, St. Andrews, Fife KY16 9ST, UK
[b] Diamond Light Source, Harwell Science and Innovation Campus, Didcot, Oxfordshire OX11 0DE, UK
[c] Aix Marseille Univ. – CNRS, Lab Chim Provence, UMR 6264, F-13331 Marseille 3, France
[d] Univ. Caen, CNRS, ENSICAEN, Catalyse & Spectrochim Lab, F-14050 Caen, France
[e] POSTECH, Dept. Chem. Engn., Pohang 790784, South Korea

ARTICLE INFO

Article history:
Received 17 March 2011
Received in revised form 17 April 2011
Accepted 20 April 2011
Available online 7 May 2011

Keywords:
Microporous silicoaluminophosphate
Copper cyclam co-template
Cu SAPO STA-7
Structure analysis
Selective catalytic reduction NO

ABSTRACT

Copper cyclam (cyclam = 1,4,8,11-tetraazacyclotetradecane) and tetraethylammonium (TEA^+) act as co-templates for the hydrothermal crystallisation of the silicoaluminophosphate SAPO STA-7, as determined by UV–visible, ESR and solid-state MAS NMR spectroscopies, powder and single crystal X-ray diffraction and chemical analysis. Calcination of the as-prepared solid in flowing oxygen removes all organics to leave Cu(II),H-SAPO STA-7 (hereafter Cu-SAPO STA-7) in which the presence of bridging hydroxyl groups is confirmed by IR and the presence of multiple environments for Cu^{2+} is shown by IR using NO as a probe molecule. Rietveld analysis of synchrotron X-ray powder diffraction data collected over the temperature range 293–673 K locates Cu^{2+} cations distributed over four sites: above six membered rings (6MRs) and in the three different 8MR windows of the STA-7 structure. Cu-SAPO STA-7 is a very good catalyst for the selective catalytic reduction of NO with NH_3, in the presence or absence of water vapour, so that this approach represents an efficient and effective route to copper-containing SAPO catalysts that obviates the need for an aqueous Cu^{2+} ion exchange step during preparation.

1. Introduction

The high temperature combustion of fossil fuels in stationary and mobile power sources gives rise to nitrogen oxides, NO_x, which are serious atmospheric pollutants. For automobile internal combustion engines working under stoichiometric fuel:air ratios, three way catalysts permit removal of NO_x from the exhaust stream via reduction with unburnt hydrocarbons and carbon monoxide, but for engines operating under lean burn conditions and also in stationary power sources there is an excess of oxygen over fuel in the inlet mixture, so that selective catalytic reduction (SCR) of NO_x (over the reduction of oxygen) is required. One possible reductant that can be added to the exhaust or flue gas is ammonia (from added urea, for example), and the use of NH_3-SCR is already a well-established approach to NO_x removal in stationary power sources [1]. Brandenberger et al. have quite recently comprehensively reviewed the SCR of NO_x by ammonia [2].

Copper-exchanged ZSM-5 zeolite was reported by Iwamoto in 1986 to be a good catalyst for direct SCR of NO_x with hydrocarbons in vehicle emissions [3] and has since been studied extensively for this reaction and also for SCR with NH_3 [4–12]. The catalytic activity of the hydrogen forms of these zeolites prior to Cu^{2+} exchange has been shown to be much lower than that of copper-containing materials, indicating the importance of the copper cations [2,12]. One mechanistic interpretation has the active site for this reaction as Cu^{2+}–Cu^{2+} dimers arranged to be able to dissociatively chemisorb NO prior to reaction [13–15]. Copper-exchanged zeolites with the chabazite structure (CHA topology) have also been shown to be active catalysts for NH_3 SCR of NO, with higher activity than Cu ZSM-5 at low temperatures, extended ranges of high NO conversion and improved structural stability compared to Cu-ZSM-5 [16,17]. Structural studies of SSZ-13 (synthetic, high silica chabazite [18]) and the structurally-related zeolite Cu-SSZ-16 [19] – show that in the activated forms of the zeolites the Cu^{2+} cations occupy three-coordinated sites within the plane of the six membered rings (6MRs) of the double six membered ring building units (D6Rs) of the chabazite structure [20]. Recently, Korhonen et al. have studied

* Corresponding author. Tel.: +44 1334 463793; fax: +44 1334 463808.
E-mail address: paw2@st-andrews.ac.uk (P.A. Wright).

1387-1811/$ - see front matter © 2011 Elsevier Inc. All rights reserved.
doi:10.1016/j.micromeso.2011.04.039

the structure of ion-exchanged Cu-SSZ-13 after dehydration and have located Cu^{2+} ions occupying the 3-fold coordinated sites next to the 6MRs [21]. Furthermore, in situ UV–visible spectroscopy indicates that during NH_3 SCR of NO over this material the copper remains in the form of isolated mononuclear Cu^{2+} species. Additionally, copper-exchanged forms of the silicoaluminophosphate (SAPO) analogue of chabazite (Cu-SAPO-34) have been shown to be active for the SCR of NO with hydrocarbons such as propene and with NH_3 [12,22,23]. Indeed, Cu-SAPO-34 has been observed to show remarkable thermal stability under reaction conditions, even in an atmosphere containing appreciable H_2O. For these studies Cu-SAPO-34 was prepared by aqueous ion exchange of calcined SAPO-34 with solutions containing Cu^{2+}(aq), giving partially ion exchanged Cu,H-SAPO-34 materials.

Here we report the synthesis and characterisation of copper-containing SAPO STA-7, prepared using a copper-cyclam complex (cyclam = 1,4,8,11-tetraazacyclotetradecane) as a structure directing agent (SDA), or 'template', in combination with tetraethylammonium (TEA^+) hydroxide. The framework of SAPO STA-7 [24–29], like that of SAPO-34, is built entirely from double six-membered ring (D6R) units, but with a different stacking arrangement that leads to a structure that has two different kinds of cages, with different sizes, small 'A' and large 'B' (Fig. 1a and b). The pore space is three dimensionally connected, with windows with free diameters (measured from the crystal structure) of: 3.2 Å between A cages, along [0 0 1]; 4.1 Å between B cages, along [0 0 1]; and 3.6 × 3.9 Å between A and B cages, along <1 0 0>. A 'co-templating' approach has previously been reported for the synthesis of SAPO STA-7 [25,27–29], where cyclam and TEA^+ were found to direct its crystallisation by templating the larger 'B' and smaller 'A' cages present in its structure. Here we show that copper-cyclam and TEA^+ cations can act as co-templates for the two different cage types in the STA-7 structure, and establish the framework chemistry and the integrity of the complex.

The use of metal-amine complexes as SDAs for aluminophosphate zeotypes has been reported previously. Rajic et al. have synthesised a variant of the aluminophosphate AlPO-34 (CHA) with $[Ni(en)_3]^{2+}$ (en = ethylenediamine) although the metal complex becomes covalently bonded to the framework [30]. Garcia et al. have shown that $[Ni(deta)_2]^{2+}$ (deta = diethylenetriamine) can direct the crystallisation of aluminophosphate AlPO(F)-34 and an orthorhombic variant of AlPO-5 in the presence of fluoride and AlPO-5, MgAPO-34 and SAPO-34 in the absence of fluoride [31,32]. Furthermore, Garcia et al. have also shown that the silicoaluminophosphate SAPO STA-6 [33] can be prepared using the nickel-tetramethylcyclam complex as an SDA.

Direct syntheses using copper amines as complexes have also been reported: the aluminophosphate-fluoride form of STA-6 has been prepared with copper-cyclam as an SDA [34], and the aluminophosphate hydroxide $AlPO_4$-21 has been prepared with the $[Cu(en)_2]^{2+}$ complex as a charge balancing template [35], but this is the first report of a SAPO templated by a copper–amine complex. As is also the case for Ni^{2+}, the location of Cu^{2+} in tetrahedral framework cation sites is not favoured in aluminophosphates and the divalent Cu^{2+} cation is strongly complexed by cyclam.

Calcination of the as-prepared solid liberates Cu^{2+} from the complex, resulting in microporous Cu,H-SAPO STA-7 (hereafter Cu-SAPO STA-7), in which the negative framework charge is balanced by Cu^{2+} and H^+ cations. This preparation route has the advantage of avoiding the additional aqueous Cu^{2+} exchange and drying steps previously used to give Cu-SAPO catalysts, and also reduces the negative effects of hydrolysis of the structure associated with this process. The Cu-SAPO STA-7 is characterised by adsorption, X-ray diffraction and MAS NMR, IR, ESR and UV–visible spectroscopy, and the accessibility of the copper cations is probed by IR in combination with the adsorption of CO and NO as probe molecules. In addition, it has been shown to be active in the SCR of NO in the presence of propene or ammonia, with particularly promising results achieved for NH_3 SCR in the presence or absence of H_2O.

2. Experimental

2.1. Synthesis and preparation

Samples of copper-containing SAPO STA-7 (designated Cu SAPO STA-7) were prepared from silicoaluminophosphate gels by the addition of two SDAs, the copper cyclam complex and tetraethylammonium ions. Replacement of cyclam by Cu^{2+}(cyclam) acetate in the preparation that gives SAPO STA-7 [25,28] was found to give a purple crystalline solid later identified as Cu SAPO STA-7. In a typical preparation, fumed silica was added to an aluminophosphate gel prepared by mixing $Al(OH)_3$ with H_3PO_4 (85%) in water, followed by addition of the copper cyclam complex, pre-prepared by adding cyclam to an aqueous solution of copper acetate. Finally a solution of tetraethylammonium hydroxide was added to give an

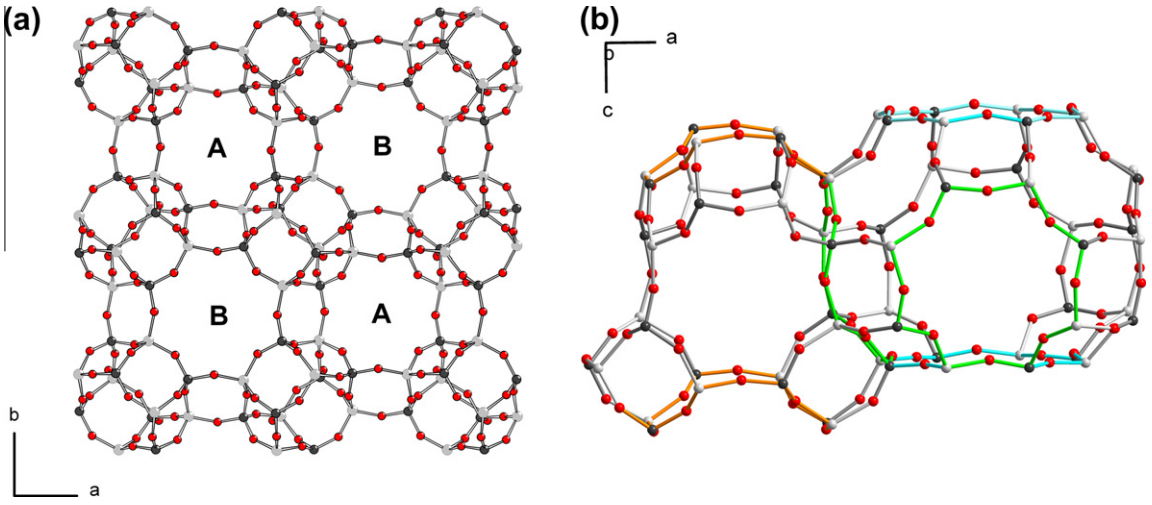

Fig. 1. Representations of the framework structure of STA-7, viewed: (a) down the *c* axis, labelling the smaller A and larger B cages and (b) along the *b* axis showing the A and B cages connected, with the three different 8MR windows outlined (A–A, orange; A–B, green; and B–B, cyan). (For interpretation of the references to colour in this figure legend, the reader is referred to the web version of this article.)

initial pH of 7. The overall gel composition was $Al(OH)_3$: 0.8 H_3PO_4: 0.2 SiO_2: 40 H_2O: 0.1 Cu(cyclam)$(OAc)_2$: 0.2 TEAOH. The gel was stirred until homogeneous, loaded into a Teflon-lined stainless steel autoclave and heated in the oven for 5 days at 463 K. The resultant product was suspended in water and sonicated to force separation of crystalline from amorphous solid, which was removed by decanting. The final crystalline product was filtered off, washed with distilled water and dried at 333 K. In order to prepare Cu SAPO STA-7 with small particle size for catalytic testing, the same preparation was repeated but with the addition of a small amount of finely ground seed crystals of as-prepared Cu SAPO STA-7. SAPO STA-7 without copper was prepared according to the published method for the purpose of comparison. In each case phase identification was achieved by laboratory powder XRD.

Thermogravimetric analysis of as-prepared solids was performed under flowing air, using a heating rate of 5 K/min. On the basis of the TGA results, conditions were chosen to remove all organics from the solids prior to characterisation of the porous solids. Calcination was then performed in flowing O_2 at temperatures between 673 and 823 K for 12 h, giving Cu-SAPO STA-7.

For comparison of catalytic performance, Cu-SAPO STA-7 was also prepared by aqueous ion exchange. As-made SAPO STA-7 with Si/(Si + Al + P) = 0.12 was prepared following the procedure described elsewhere [25,28] and calcined in air at 823 K for 10 h to remove organic SDAs. Then, the calcined SAPO samples were exchanged with 0.01 M Cu^{2+} acetate aqueous solution at room temperature for 6 h. At the final stage of Cu^{2+} ion exchange, several drops of ammonia water (26%, DC) were added to adjust the pH of the solution containing SAPO powder to 7.5. After Cu^{2+} ion exchange, when necessary, the resulting solids were calcined in air at 823 K for 4 h. In order to distinguish between the directly synthesised and ion-exchanged Cu-loaded molecular sieves in the catalytic tests, the suffix "DS" or "IE" is attached in parentheses to their general names when discussing the catalytic results.

Finally, NH_4^+-ZSM-5 with Si/Al = 14 was obtained from Tosoh and exchanged with Cu^{2+} as described above to compare catalytic performance.

2.2. Characterisation

Laboratory powder X-ray diffraction of as-prepared and calcined samples of Cu SAPO STA-7 were performed in Debye–Scherrer mode using 0.7 mm sealed quartz glass capillaries on a STOE STADI/P diffractometer (Cu $K_{\alpha 1}$, 1.54056 Å) to establish crystallinity and purity.

Scanning electron microscopy of Cu SAPO STA-7 was performed on a JEOL JSM-5600 SEM with an Oxford INCA Energy 200 EDX analyser to determine the Cu, Si, Al and P content: samples were ground fine prior to analysis, to minimise the effects of zoning on the measured compositions. Additional elemental analysis for Si, Al, P, and Cu was carried out using a Jarrell-Ash Polyscan 61E inductively coupled plasma spectrometer in combination with a Perkin–Elmer 5000 atomic absorption spectrophotometer. Carbon, hydrogen and nitrogen analysis was performed on as-prepared samples using a CEA 1110 CHNS Analyser. X-ray photoelectron spectra (XPS) were recorded on an ESCALAB 220-IX spectrometer with a Mg K_α X-ray source (1253.6 eV). Typically, five scans were accumulated and all binding energies are referenced to the C(1*s*) line at 284.6 eV from adventitious carbon. Surface Cu/Al or Cu/Si ratios were calculated from the Cu($2p_{3/2}$) and Al(2*p*) or Si(2*p*) line intensities using approximate sensitivity factors. In addition, the concentration and location of copper in calcined Cu SAPO STA-7(DS) and Cu exchanged Cu-SAPO STA-7(IE) were examined under a JEOL JEM-2010 transmission electron microscope (TEM) operating with an acceleration voltage of 200 kV. Although this resulted in the reduction of Cu^{2+} to copper metal, it does reveal details of the Cu^{2+} distribution in the two solids.

Solid-state NMR experiments were performed using a Bruker Avance III 600 spectrometer, equipped with a widebore 14.1 T magnet, yielding Larmor frequencies of 243.0 MHz for ^{31}P, 119.2 MHz for ^{29}Si, 156.4 MHz for ^{27}Al and 150.9 MHz for ^{13}C. Samples were packed in conventional 1.3 or 4 mm ZrO_2 rotors and rotated at a rate of either 60 kHz (1.3 mm rotors) or 10 kHz (4 mm rotors). Chemical shifts are recorded in ppm relative to 85% H_3PO_4 for ^{31}P, 1 M $Al(NO_3)_3$ (aq) for ^{27}Al and TMS for ^{29}Si and ^{13}C. All spectra were recorded with a Hahn-echo pulse sequence and a repeat interval of either 20 ms (^{29}Si, ^{13}C) or 500 ms (^{31}P, ^{27}Al) and a 1 MHz spectral width. Signal averaging was carried out over 64 transients (^{31}P), 24576 transients (^{29}Si), 128 transients (^{27}Al) and 1048576 transients (^{13}C).

The porosity of the calcined solids was established by the measurement of adsorption isotherms for N_2 at 77 K measured gravimetrically on a Hiden IGA instrument or volumetrically using a Micromeritics Tristar or a Mirae SI nanoPorosity-XG analyser.

IR spectroscopy was performed in transmission mode on calcined samples of Cu SAPO STA-7 and SAPO STA-7. Spectra were measured at room temperature on self-supporting wafers (~30 mg, 2 cm^2) placed in a quartz cell with KBr window. They were recorded at room temperature with a Nicolet Nexus spectrometer accumulating 128 scans at a spectral resolution of 4 cm^{-1}. The infrared cell was connected to a vacuum line for evacuation and dehydration. Two types of probe molecule were used to examine adsorption sites in the solids, NO and CO: initially FTIR of CO was performed to identify the presence of any Cu^+ and subsequently NO was used as a probe molecule because of its strong and characteristic interaction with Cu^{2+} [36–40]. In each case samples were measured after dehydration by heating at 573 K under vacuum and also, in most cases, after a subsequent thermal treatment at 573 K for 4 h in 67 mbar of O_2 followed by cooling to 393 K and then room temperature evacuation. Spectra of (i) the dehydrated and (ii) the dehydrated and O_2-treated samples were used as background and subtracted from the spectra measured in the presence of adsorbed species.

UV–visible spectra of as-prepared and calcined Cu SAPO STA-7 were measured in diffuse reflectance mode on a Perkin Elmer Lambda 35 UV–visible spectrometer, on samples exposed to the atmosphere. Vividly coloured samples were mixed with $BaSO_4$. Samples were loaded in 2 mm pathlength quartz cuvettes. Data, collected as percentage reflectance over the wavelength range 300–1000 nm, were handled on the accompanying Lambda UV-Winlab software.

ESR spectra of as-prepared and calcined Cu SAPO STA-7 samples were measured at 293 K using a Bruker EMX spectrometer operating at 9.52 GHz. Calcined samples were dehydrated at 573 K under a vacuum of 10^{-4} mbar in 4 mm quartz glass tubes attached to a glass vacuum line and sealed prior to measurement. In addition to being dehydrated, samples were subsequently heated at 573 K for 4 h in 100 mbar of O_2 and re-evacuated prior to the tubes being sealed. In order to avoid saturation of the resonance line, low microwave power was employed (typically between 0.4 and 4 mW). Hyperfine constants were measured using WinEPR software and $g_{||}$ values were calculated.

2.3. Crystallography

2.3.1. Single crystal diffraction

Single crystal diffractometry was performed using a Rigaku diffractometer with a CCD detector using Mo K_α X-radiation (from a rotating anode) on large crystals of Cu SAPO STA-7 of 60 μm dimensions in the as-prepared state (purple), calcined at 673 K in O_2 for 12 h (green) and calcined at 823 K in O_2 for 12 h (turquoise).

Table 1
Single crystal diffraction details for Cu SAPO STA-7 in as-prepared and calcined forms.

	As-prepared Cu SAPO STA-7	Cu-SAPO STA-7 (calc, 823 K)
Unit cell composition (refined)	$Cu_{1.2}(cyclam)_2(TEA^+)_2$ $Al_{24}Si_6P_{18}O_{96}\cdot xH_2O$	$Cu_{1.2},H_{3.6}Al_{24}Si_6P_{18}O_{96}\cdot xH_2O$
Unit cell weight	3666.6	3007.4
Calc. density/g cm^{-3}	1.861	1.565
Temperature/K	93(2)	93(2)
Space group	*P* 4/*n*	*P* 4/*n*
X-ray source	Rotating anode Mo K_α	Rotating anode Mo K_α
Wavelength/Å	0.71073	0.71073
Unit cell/Å	*a* = 18.668(2)	*a* = 18.487(3)
	c = 9.3863(17)	*c* = 9.336(3)
Volume/Å^3	3271.2(8)	3190.7(12)
R_F (all data)	0.0827	0.161
R_F ($I > 2\sigma I$)	0.0780	0.147
Max and min residual e-density/e Å^{-3}	−1.2, 1.7	−0.5, 1.9

In both calcined materials, analysis of the bulk sample showed that no organic remained. In each case, the framework structure was solved and refined using SHELXTL [41] in space group P4/n, as observed previously for SAPO STA-7 [25], which allows for Al – (P,Si) order in framework sites. Additional extra framework electron density observed from Fourier mapping was refined as C, N (and Cu) atoms of SDAs and the O of water molecules (in the as-prepared solid) or as Cu^{2+} cations and/or water O atoms (in the calcined solids).

For the as-prepared solid, extra framework density in the smaller cage of STA-7 was refined as N and C atoms of the TEA^+ cation, disordered over two equivalent orientations, but with one cation per cage. Within the large cage, the difference Fourier analysis clearly revealed the location of the copper-cyclam complex, although the cyclam ring showed disorder as a result of the 4-fold symmetry of the site. The most reasonable combination of occupancy and displacement parameter for the Cu^{2+} was achieved with 0.6 Cu per large cage (1.2 Cu^{2+} per unit cell). Although this was a little lower than that calculated by EDX analysis of this material, ground fine (1.8 Cu^{2+} per unit cell) it may be that these largest crystals were not fully representative of the bulk. Finally, some extra framework scattering in the centre of 8MR windows between the larger cages was attributed to water molecules. See Table 1 and Supplementary Data for crystallographic details.

For the calcined crystals, no special measures were taken to prevent the adsorption of water, so that it was not possible to distinguish between Cu^{2+} cations and O atoms of water molecules. No significant differences in the position of extra-framework scattering were observed between the refined structures of samples calcined at 673 and 823 K, so that only the second structure is reported here. The data is of significantly lower quality than that obtained for the as-prepared material, leading to higher residuals, presumably due to lack of crystal quality during calcination. Nevertheless, extra framework scattering attributed to hydrated Cu^{2+} cations 3.0–3.5 Å from framework O atoms was located nearby 6MRs and in 8MRs between large cages and also in 8MRs between large and small cages. See Table 1 and Supplementary Data for crystallographic details.

2.3.2. Powder diffraction

Synchrotron X-ray powder diffraction was performed on a sample of Cu-SAPO STA-7 that had been calcined at 823 K, loaded into a 0.5 mm quartz glass capillary, dehydrated, pre-treated in O_2 at 573 K and finally evacuated at 393 K at 10^{-4} mbar before being sealed. The sample was examined in Debye–Scherrer geometry at station I-11 of the Diamond Light Source Synchrotron [42], using X-rays of wavelength 0.825028 Å. To minimise the effects of beam damage, eight data sets were collected for three minutes each over the range 1–140° 2θ, with a fresh portion of the sample exposed to the beam by translating the capillary between collections. The eight data sets were summed and binned on a 0.002° step size. Data at 2θ angles greater than 50° were discarded, as the intensity of the peaks strongly decreased. Finally, the data were re-binned to a step size of 0.003°. Diffraction patterns were collected at temperatures between 293 and 673 K, controlled by a hot air blower.

Rietveld refinement of the instrumental parameters and the Cu SAPO STA-7 structure against the diffraction profiles was performed using the GSAS suite of programs [43], using the single crystal structure of calcined SAPO STA-7 as a starting model for the calcined material, with 25% occupancy of the three P sites by Si. The profile was modelled using a pseudo-voigtian function and the background was modelled using a 36 term cosine function. The framework Al–O and (P,Si)–O distances were constrained during refinement to 1.73(2) and 1.52(2) Å, respectively, and O–O distances were constrained to 2.82(5) Å (for AlO_4 tetrahedra) and 2.49(5) Å for $(P,Si)O_4$ tetrahedra. Difference Fourier analysis and iterative refinement of positions and occupancies were used to locate extra framework Cu^{2+} cations at four partially-occupied sites. In the final refinement cycle only the fractional occupancies of these four sites (as well as the framework atomic coordinates) were refined.

For Cu-SAPO STA-7 at 293 K, the Rietveld fit is given in Fig. 2, and the crystallographic parameters are given in Table 2 and in the Supplementary Information. Similarly good fits to the data were achieved using the same refinement procedure for the samples examined at 473, 573 and 673 K, and crystallographic details are given in Table 2.

2.4. NO SCR

All the catalytic experiments were conducted at atmospheric pressure in a conventional continuous-flow microreactor. Around 1 g of the catalyst was sieved to a mesh size of 20/30 to minimise the mass transfer limitations. Before the evaluation of activity, the catalyst was pre-treated in situ with a total flow of 3300 cm^3 min^{-1} containing 79% N_2 and 21% O_2 (for Cu SAPO STA-7(DS)) or 100% N_2 at 773 K for 2 h (for ion-exchanged Cu-ZSM-5(IE) or Cu-SAPO STA-7(IE)) and then cooled to room temperature. A model reaction gas mixture consisting of 500 ppm NO, 500 ppm NH_3 or 2000 ppm C_3H_6, and 5% O_2 with or without 10% H_2O in N_2 balance was fed into the reactor system. A total flow rate of 3300 cm^3 min^{-1} (100,000 h^{-1} GHSV) was used for the catalyst activity testing. The inlet and outlet gas compositions were monitored by a Nicolet 6700 FT-IR spectrometer equipped with a gas cell.

3. Results and discussion

3.1. Synthesis and structure of as-prepared Cu SAPO STA-7

Addition of the copper-cyclam complex and tetraethylammonium hydroxide to the SAPO gel, followed by hydrothermal treatment at 463 K for 5 days gives the SAPO STA-7 structure, as shown by laboratory X-ray powder diffraction (Supplementary Data). The pattern was successfully indexed using Visser's algorithm on a tetragonal cell, *P* 4/*n*, *a* = 18.732(3) Å, *c* = 9.401(2) Å, figure of merit 38, similar to that reported previously for SAPO STA-7. SEM indicates that the average crystal sizes are in the range 20–60 μm, according to the batch (Fig. 3). Many show a complex morphology in which the individual STA-7 crystals appear to

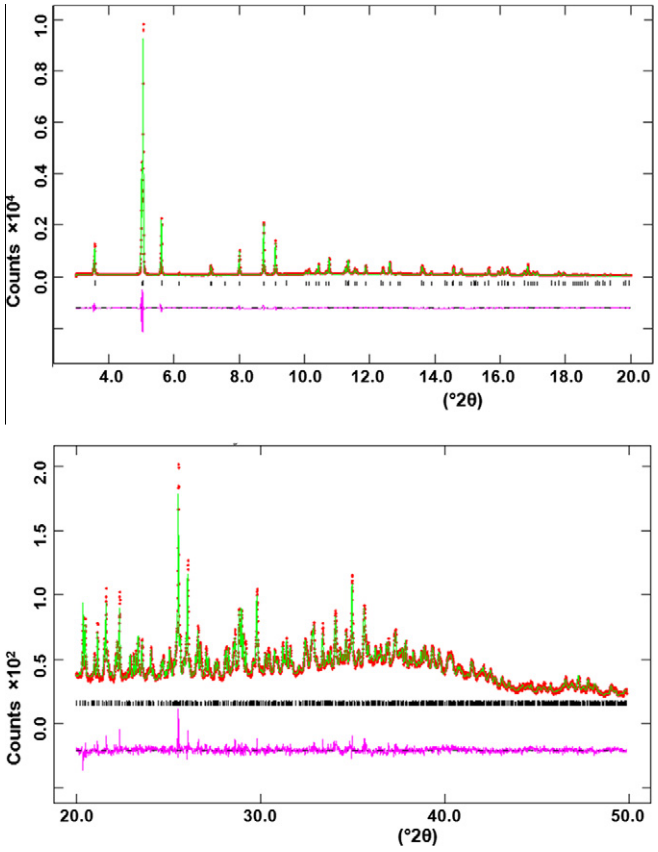

Fig. 2. Rietveld profile fit to synchrotron X-ray powder diffraction data collected at 293 K on Cu-SAPO STA-7 prepared by calcination of as-prepared Cu SAPO STA-7 at 823 K in oxygen. (λ = 0.825028 Å, P 4/n, a = 18.65727(13) Å, c = 9.41009(9) Å, R_{wp} = 0.071, R_p = 0.055).

include intergrown crystallites related by a 90° rotation of the tetragonal (c-) axis. This type of intergrowth is not observed for SAPO STA-7 prepared without the inclusion of copper in the cyclam, in which case the crystals exhibit simple tetragonal prismatic shape, and is likely to arise from the effect of the copper cyclam complex in cont rolling the stacking of layers of D6Rs [27].

The copper cyclam complex retained its bright purple colour in the gel and in the resultant product SAPO, indicating that the complex is both stable under hydrothermal conditions and incorporated into the product phase. The UV–visible reflectance spectrum of the as-prepared material (Supplementary Data) shows a broad maximum at around 500 nm, characteristic of this complex (λ_{max} = 508 nm) [44]. The ESR spectrum of the as-prepared material is shown in Fig. 4. Due to overlap of the parallel and perpendicular regions, the spectrum only shows two absorptions in the parallel region and a characteristic 'overshoot' peak in the perpendicular region. Nevertheless, it is possible to measure $A_{||}$ and to calculate $g_{||}$ as 206 G and 2.18, respectively, values that very similar to those ($A_{||}$, 206 G; $g_{||}$, 2.19) of the similar square planar Cu(II)-cyclam$(H_2O)_2$ [45] and are typical of axially symmetric Cu(II) complexes with the unpaired electron in the d_{x2-y2} orbital. These data confirm the inclusion of copper complexed by cyclam within SAPO STA-7.

Solid-state MAS NMR of as-prepared Cu SAPO STA-7 gives good quality ^{31}P, ^{29}Si, ^{27}Al [46] and reasonably well defined ^{13}C spectra (Fig. 5a–d), indicating that the Cu^{2+} complex, whilst paramagnetic, does not strongly broaden all the resonances. The ^{29}Si MAS NMR spectrum has a single broad peak at −91.9 ppm, corresponding to Si$(OAl)_4$, which indicates that the Si substitutes into the lattice mainly by the Si ↔ P mechanism and that the different crystallographic sites of the STA-7 structure are not resolved by this technique. The ^{27}Al MAS spectrum shows two peaks, a major one at 38.7 ppm and a minor one at 9.3 ppm. The peak at approximately 38.7 ppm is characteristic of tetrahedral Al in AlPOs, whereas the peak at 9.3 ppm is due to 5-fold Al in which an extra-framework species such as OH, or H_2O increases the coordination. The ^{31}P MAS NMR of the as-synthesised material shows a single peak at −29.1 ppm, characteristic of tetrahedral P$(OAl)_4$. The ^{13}C spectrum of the as-synthesised material shows a relatively sharp peak at 9.2 ppm, attributed to the methyl carbon of TEA^+ and a broader peak at approximately 55 ppm assigned to the methylene carbon of TEA^+ [47]. The broad feature between 15 and 40 ppm is assigned to the Cu-cyclam complex, broadened by the presence of complexed Cu^{2+}. This ^{13}C MAS NMR, combined with UV–visible and ESR spectroscopy indicates that both Cu-cyclam and TEA^+ are present as co-templates in the as-prepared material, as is the case for cyclam and TEA^+ in SAPO STA-7.

Table 2
Rietveld refinement details for variable temperature synchrotron X-ray powder diffraction studies of Cu-SAPO STA-7 calcined at 823 K (I11, Diamond Light Source, λ = 0.825028 Å, space group P 4/n).

Temperature/K	293	473	573	673
2θ range	2–50	2–50	2–50	2–50
R_{wp}, R_p	0.071, 0.055	0.065, 0.054	0.067, 0.054	0.067, 0.054
Ls shift/esd. (max, min)	0.04, 0.01	0.02, 0.01	0.03, 0.01	0.03, 0.01
Max. and min. residual e-density/e Å^{-3}	0.55, −0.7	1.0, −1.1	1.0, −0.9	0.4, −0.3
Cell parameters/Å	a = 18.65727(13) c = 9.41009(9)	18.64178(15) 9.39621(10)	18.63380(17) 9.38838(11)	18.62143(14) 9.37824(10)
Unit cell volume/Å^3	3275.59(7)	3265.33(8)	3259.82(8)	3251.97(7)
Cu1(obs)/unit cell^{-1}	0.54(2)	0.59(2)	0.68(2)	0.82(2)
Cu2(obs)/unit cell^{-1}	0.37(2)	0.38(2)	0.34(2)	0.32(2)
Cu3(obs)/unit cell^{-1}	0.37(2)	0.43(2)	0.34(2)	0.43(2)
Cu4(obs)/unit cell^{-1}	0.18(2)	0.29(2)	0.23(2)	0.16(2)
∑Cu(obs)/unit cell^{-1}	1.46	1.69	1.59	1.73

TGA analysis shows a weight loss up to 573 K attributed to water: for the as-prepared Cu SAPO STA-7 studied by MAS NMR, this weight loss was around 5% (Fig. 6). The major weight loss, of ca. 17.5%, occurred between 573 and 873 K, with a maximum rate of mass loss at around 773 K. This corresponds to complete removal of organics from the solid, leaving a turquoise solid. Combining elemental, EDX, TGA, and MAS NMR analyses, and charge balancing, gives an elemental composition of $(CuL)_{1.8}$ $(NC_8H_{20})_2$ Al_{24} $Si_{5.6}$ $P_{18.4}$ O_{96} $\cdot 11H_2O$ (L = cyclam); Calc. C 10.6%, H 2.7%, N 3.4%; Exp. C 10.4%, H 2.49%, N 3.30%.

Single crystal diffraction studies of as-prepared Cu SAPO STA-7 show that the copper cyclam complex is located in the larger cages and the tetraethylammonium ion is found to occupy the smaller cages, where it adopts the tg.tg configuration (Fig. 7). The location of the cyclam complex is consistent with what was previously observed for the nickel tetramethylcyclam complex in Ni CoAPO STA-7 [33] and the configuration of the TEA^+ is as previously observed for SAPO STA-7 [25]. The copper cyclam complex and TEA^+ therefore act as co-templates for SAPO STA-7 synthesis. Together, the charge on these co-templates matches the negative framework charge on the SAPO STA-7 that arises from the substitution of Si on P sites in the framework that is shown by MAS NMR.

For catalytic testing, smaller crystallite size was required. Seeding preparations gave small cuboidal crystals with a particle size of

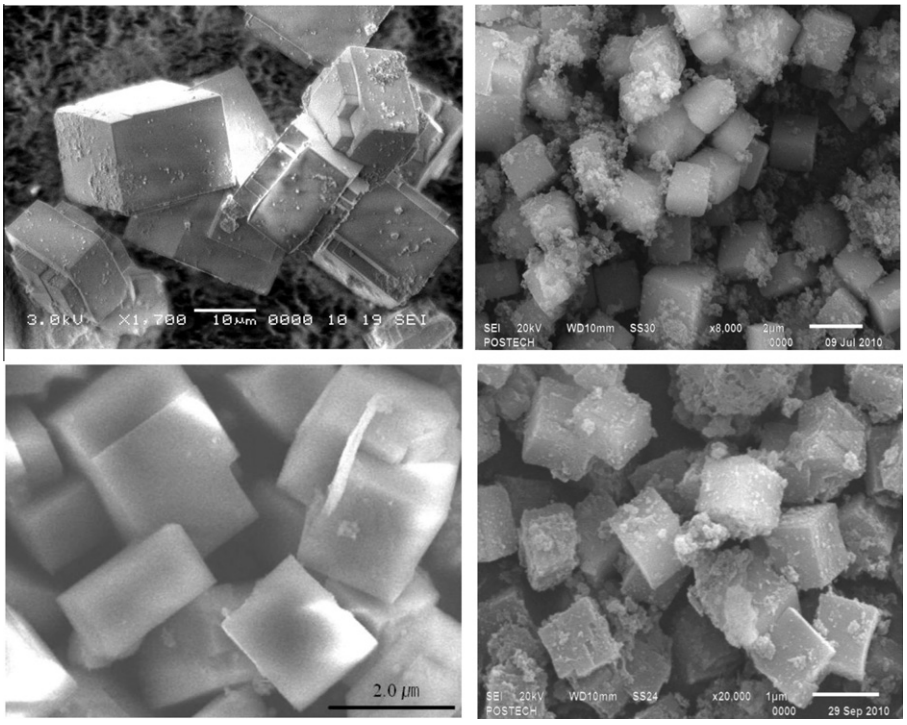

Fig. 3. SEM of (above left) as-prepared Cu SAPO STA-7 (via use of copper cyclam co-template), large crystals; (above right) Cu SAPO STA-7, small crystals prepared with cyclam complex by seeding; (below left) SAPO STA-7, small crystals; (below right) Cu-SAPO STA-7 prepared by aqueous ion exchange of calcined small crystals of SAPO STA-7.

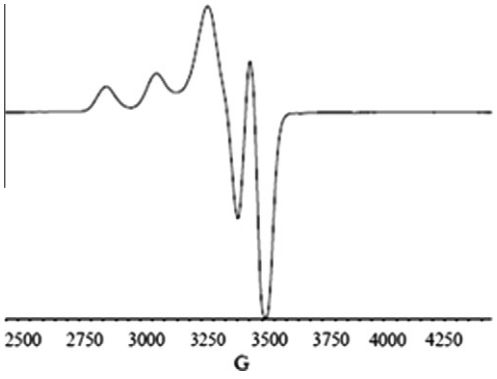

Fig. 4. ESR spectrum of as-prepared Cu-cyclam containing SAPO STA-7.

around 3 μm. PXRD indicated the crystalline product was phase-pure Cu SAPO STA-7, but SEM indicated that minor amounts of amorphous material were also present. Selected area EDX analysis indicated that the inorganic (Cu, Si, Al, P) content of these small crystals was similar to that observed for the larger crystals characterised in more detail and described above.

3.2. Structure of calcined Cu-SAPO STA-7

On the basis of the TGA results, as-prepared samples of Cu SAPO STA-7 were calcined for 12 h in flowing O_2 at 673 and 823 K. This removes all organic material from the pores, as confirmed by elemental analysis: after heating at 673 K the sample is green, whereas after heating at 823 K it is light blue or turquoise. Crystallinity is retained (Supplementary Data). Diffuse reflectance UV–visible spectroscopy of Cu SAPO STA-7 calcined at 823 K (Supplementary Data) gives a broad absorption centred at 800 nm, characteristic of Cu^{2+} coordinated by oxygen (cf. Cu^{2+}(aq), λ_{max} = 780 nm) [48]. As stated earlier (and described in the Supplementary Data), single crystal diffraction studies of samples calcined at 673 and 823 K and exposed to moisture were able to locate extra framework scattering density in three sites, each around 3 Å from framework O atoms and attributed to hydrated Cu^{2+} cations.

The calcined Cu-SAPO STA-7 was subsequently dehydrated under vacuum and examined by infrared spectroscopy to investigate the nature of the copper species prepared in this way. Two molecular adsorbates were used as IR probes, CO and NO. Whereas CO only chemisorbs strongly on Cu^+ at room temperatures, NO adsorbs on both Cu^+ and Cu^{2+} (more strongly on the divalent ion) with the IR frequency of the adsorbed species strongly dependent on the cationic charge [36]. Dosing CO at low partial pressure on calcined Cu-SAPO STA-7 heated in vacuum at 573 K for 3 h and subsequently cooled to room temperature initially showed an absorption at 2156 cm^{-1}, attributed to Cu^+–CO. With increased loading of CO two new bands were observed at 2176 and 2147 cm^{-1}, attributed to $Cu^+(CO)_2$ (Supplementary Data). Whereas these two bands disappeared upon subsequent evacuation at room temperature, the former band, corresponding to CO bound to Cu^+ was only removed by evacuation above 423 K. IR spectroscopy was also performed on a sample of Cu SAPO STA-7 treated in a similar way to that described above, but using NO rather than CO as the probe molecule. In this case, two absorption bands were observed from the first doses: a broader, complex band from 1960 to 1840 cm^{-1}, attributed to Cu^{2+}-NO species and a second, narrower resonance at around 1805 cm^{-1}, attributed to Cu^+-NO (Supplementary Data).

Taken together, these data indicate the presence of an appreciable concentration of Cu^+. To determine whether this results from the evacuation, a sample was treated in O_2 at 573 K and cooled under O_2 prior to evacuation. Subsequent dosing of NO using the same conditions as before again gave a complex band at 1960–1840 cm^{-1}, but very weak absorbance at the wavenumber, 1805 cm^{-1}, typical of Cu^+-NO. Furthermore, dosing of CO on a sample of Cu-SAPO STA-7 prepared by heating in O_2 prior to evacuation

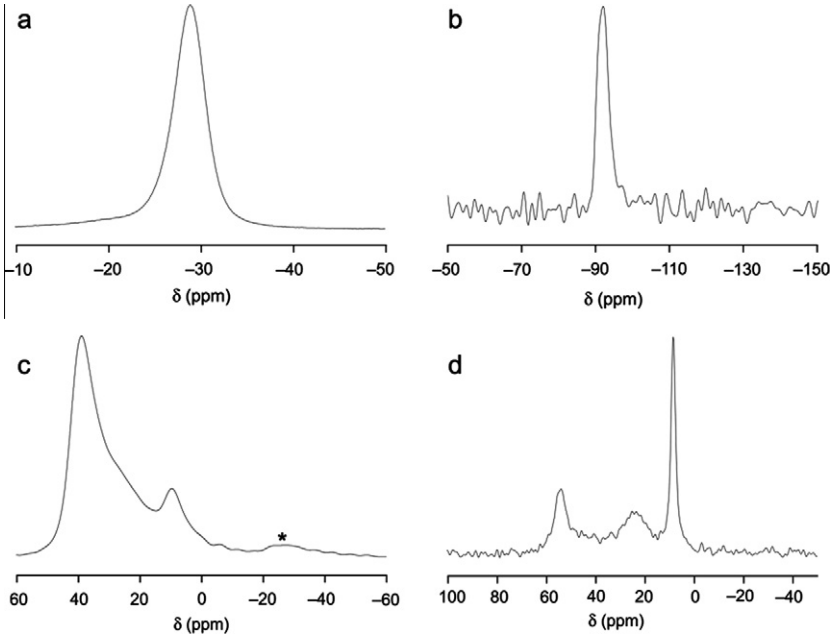

Fig. 5. Solid-state MAS NMR spectra for as-prepared Cu SAPO STA-7: (a) ^{31}P, (b) ^{29}Si, (c) ^{27}Al (spinning sideband denoted with an asterisk), (d) ^{13}C. No resonances were observed outside the range shown. Details of spectral acquisition given in the text.

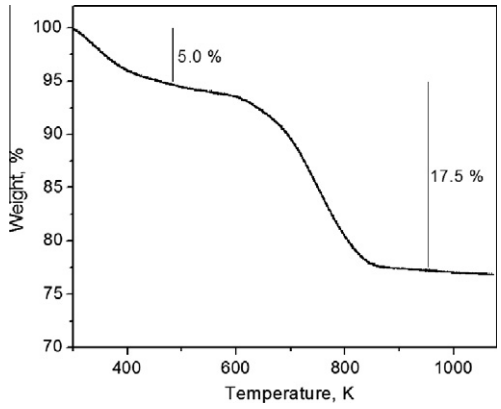

Fig. 6. TGA of as-prepared Cu SAPO STA-7 (30 μm particle size), heated at 5 K/min in flowing air.

at 393 K gave only very weak absorbance due to Cu^{+}-CO. It was therefore concluded that upon calcination of Cu SAPO STA-7 in O_2 the copper is mainly present as Cu^{2+}, but that upon subsequent dehydration under vacuum to remove physisorbed water a small but significant fraction of this Cu^{2+} became Cu^{+}. To avoid this, and therefore to enable analysis of calcined, dehydrated samples by XRD, IR and ESR, the protocol of heating at 573 K in O_2 followed by room temperature evacuation of the oxygen was adopted prior to these analyses.

Calcined Cu SAPO STA-7 treated as described above was investigated by FTIR spectroscopy. Small doses of NO (up to 50 doses per sample, each of around 0.086 μmol) were admitted sequentially onto self-supporting wafers of calcined Cu SAPO STA-7 ca. 30 mg in mass (containing ca. 15 μmol Cu^{2+}) and the IR spectra measured at room temperature. Subsequently, spectra were taken at equilibrium pressures of NO of 1.33, 2.67, 4, 5.33 and 6.67 mbar (Fig. 8). The procedure was repeated for different batches of Cu SAPO STA-7. The spectra show the development of a strong and complex absorption band from 1840 to 1960 cm^{-1} characteristic of Cu^{2+} cations in extra framework positions in SAPOs (Fig. 9), the shape of which changes with increasing addition of NO. This band can be deconvoluted into at least four absorptions, as shown in Fig. 9, corresponding to NO adsorbed onto Cu^{2+} cations in at least four different cation sites initially, and possibly five at higher loadings. Small variations in the relative intensities of these bands were observed for different Cu-SAPO STA-7 samples, but the positions of the bands were in each case similar. At the higher equilibrium pressures of NO the intensity of the Cu^{2+}-NO band continues to increase and an additional strong band develops at 2130 cm^{-1}. The assignment of this band has proved controversial, and it has been ascribed variously to NO_2 (chemisorbed), NO^{+} and N_2O [49,50]. In our opinion, the assignment to NO^{+} species [49] is the most likely, taking into account the parallel formation of water species and nitrates (bands near 1609 and 1550 cm^{-1}, respectively). Additional bands were observed at 2866, 2441 and 1609 cm^{-1}, which were due to the presence of H-bonded water.

The OH stretching region of the dehydrated solid showed two bands due to Brønsted acid bridging hydroxyl groups, at 3604 and 3625 cm^{-1} (Fig. 10). These arise because the negative charge on the framework cannot be fully balanced by Cu^{2+} cations liberated from the cyclam complex, so that protons remain after decomposition of the organic SDAs.

ESR spectroscopy of calcined Cu SAPO STA-7, pre-treated in O_2 and dehydrated, gives the spectrum shown in Fig. 11. Four strong signals are observed in the parallel region, with $A_{\|}$ 151 G and $g_{\|}$ 2.32, values that are very similar to values reported for other dehydrated Cu-containing phases (Cu-erionite, $A_{\|}$ 156 G, $g_{\|}$ 2.33; Cu-mordenite, $A_{\|}$ 154 and 161 G and $g_{\|}$ 2.33; Cu-ZSM-5, $A_{\|}$ 145 G and $g_{\|}$ 2.33) [51,52]. Closer inspection reveals a second group of signals displaced to lower Gauss, estimated $A_{\|}$ 135 G and $g_{\|}$ 2.38, of much lower intensity, which could be due to incompletely dehydrated Cu^{2+} cations.

Rietveld analysis and difference Fourier analysis of Cu-SAPO STA-7, calcined at 823 K and measured at temperatures from 293 to 673 K, identifies four sites for Cu^{2+} cations, with total occupancy estimated at 1.4–1.7 Cu^{2+} cations per unit cell, in reasonable agreement with the chemical composition estimated from EDX. This finding is also in general agreement with the observation of at least four bands in the IR experiments performed with NO as a probe –

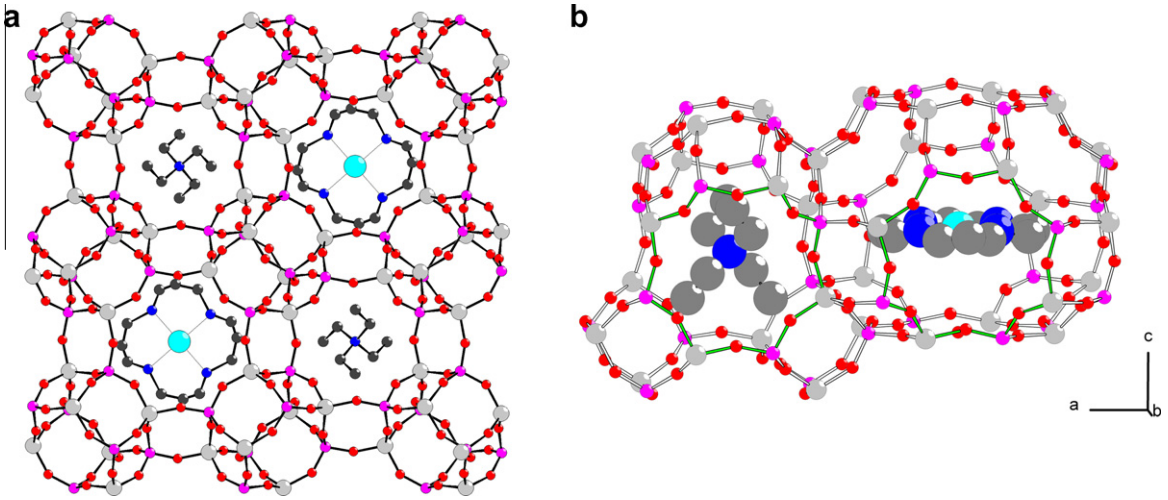

Fig. 7. As-prepared Cu SAPO STA-7, as determined from single crystal analysis, viewed: (a) down the *c* axis, and (b) along the *b* axis. One possible orientation of two is in each case shown for the copper cyclam complex and the tetraethylammonium ion. (Al atoms, grey; P atoms, pink; O atoms, red; N atoms, small dark blue; C atoms, small black; Cu(II) cations, large light blue). In (b) the 8MRs connecting small and large cages are outlined in green. (For interpretation of the references to colour in this figure legend, the reader is referred to the web version of this article.)

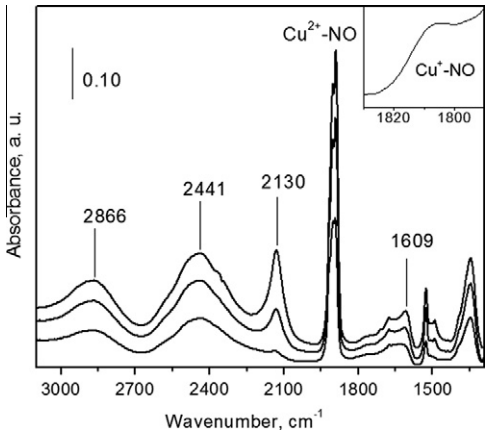

Fig. 8. FTIR spectra of NO adsorbed on activated Cu-SAPO STA-7 (573 K in O_2). Successive adsorption of equilibrium pressures: 1.33 mbar (lower), 4 mbar (middle) and 6.67 mbar (upper). The inset shows the magnification for the Cu^+-NO region for the 1.33 mbar equilibrium pressure.

no fifth site for Cu^{2+} could be located. Fig. 12 shows the distribution and Fig. 13 the local environments of these sites, Cu1 to Cu4, in agreement with the multiple adsorption sites observed upon NO introduction (ν(NO) bands of Cu^{2+}–NO complexes between 1960 and 1840 cm^{-1}).

For Cu-SAPO STA-7 at 293 K, Cu1 is located within the larger cage, close to the 6MRs that face into the cage but slightly proud of the plane of these rings, with Cu-O distances of 2.13(4), 2.42(4) and 2.48(5) Å. All other Cu sites are located in 8MR sites between cages: Cu2 is located in the 8MR window between smaller cages, disordered over four equivalent sites, where it achieves coordination with three framework O atoms (2.07(4), 2.05(4), 2.73(7) Å); Cu3 is located in the 8MR window sites between larger cages (Cu-O: 2.02(5), 2.24(4) Å); Cu4 is located in the 8MR window sites between smaller and larger cages (Cu-O: 2.07(5), 2.23(5), 2.30(5) Å). It is apparent that upon calcination at high temperature, liberation from the cyclam enables Cu^{2+} cations to migrate throughout the unit cell.

Site Cu1 is at each temperature the most populated of the sites, and there is a slight increase of the fractional occupancy of this site corresponding to an increase from 0.54 to 0.82 Cu^{2+} cations per unit cell as the temperature is increased. At higher temperatures than 293 K, the distances between Cu3 and one framework O becomes lower than physically reasonable (1.7 Å). This has been observed previously for refinements of Cu-ZSM-5 [53]. Rather than constraining the distance, we suggest that this may be explained in terms of changes in the framework in the presence of the cation that are not observed due to its low fractional occupancy (ca. 0.05).

Nitrogen adsorption measurement at 77 K on calcined samples of Cu SAPO STA-7 with both small and large particle sizes gives type I isotherms (Supplementary Data) with uptakes (at $p/p_o = 0.2$) of 18.2–21.6 wt.%, indicating internal pore volumes in the range 0.22–0.27 $cm^3\ g^{-1}$, which are comparable with that reported for SAPO STA-7 prepared without copper complexes (0.30 $cm^3\ g^{-1}$).

3.3. Catalytic characterisation and performance in the selective catalytic reduction of NO

The chemical composition, particle sizes and morphology, and pore volumes of all catalyst samples tested are given in Table 3. The catalytic conversions of NO with NH_3 as a function of reaction temperature, with and without added water, are shown in Fig. 14, along with the results of SCR with propene. No N_2O was detected during the catalytic tests and the catalysts remain crystalline after them (see Supplementary Data for PXRD of Cu-SAPO STA-7(DS) after calcination and after use in catalysis).

SCR of NO with NH_3 without H_2O shows activity at low temperatures over Cu-SAPO STA-7(DS), with conversion exceeding 80% by 473 K and 95% by 523 K, decreasing gradually with an increase in reaction temperature to 70% at 773 K. Although this conversion is slightly lower than that observed over Cu-ZSM-5(IE) at 473–543 K (which achieves 100% at 543 K) the latter catalyst loses activity more rapidly at elevated temperatures. Compared to both of these catalysts, Cu-SAPO STA-7(IE) shows a lower conversion over the complete temperature range. In the presence of H_2O, the NO SCR performance of Cu-SAPO STA-7(DS) is very similar to that of Cu-ZSM-5(IE), with slightly higher conversions below 543–613 K (when conversion over both catalysts is ca. 100%) and slightly lower conversion at higher temperatures (above 613 K). Again, the Cu-SAPO STA-7(IE) shows activity for the SCR of NO, but is less active than the other two catalysts.

The performance of the catalysts in the SCR of NO in the presence of propene was also measured. For this reaction the Cu

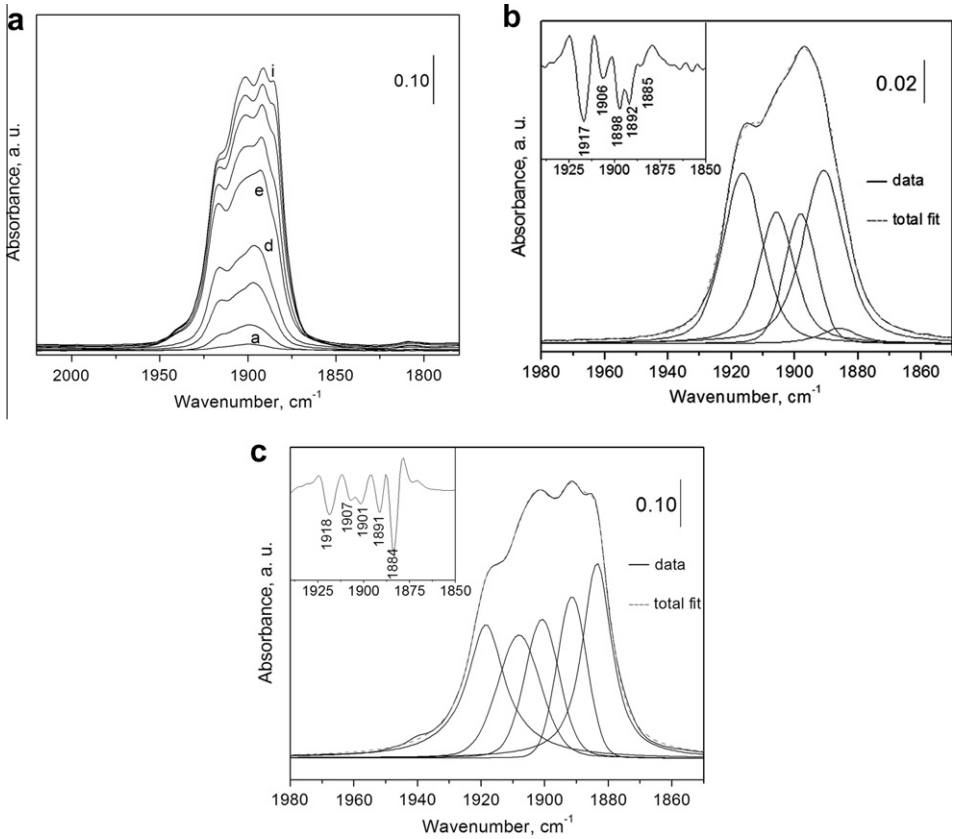

Fig. 9. FTIR spectra of NO adsorbed at room temperature on activated Cu-SAPO STA-7 (treated 573 K in O_2). (a) Spectra from successive adsorptions of: 1 (a), 5 (b), 20 (c), 50 (d) small doses of 0.086 μmol of NO and under NO equilibrium pressures of 1.33 mbar (e), 2.67 mbar (f), 4 mbar (g), 5.33 mbar (h) and 6.67 mbar NO (i). (b) Deconvolution of the spectrum (c) – with addition of 1.7 μmol NO. (c) Deconvolution of spectrum (i), under an equilibrium pressure of NO of 6.67 mbar. Second derivative spectra are inset for the last two.

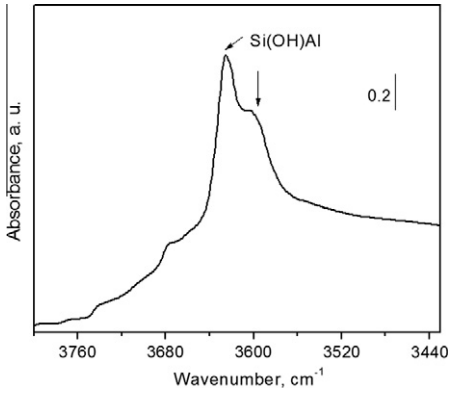

Fig. 10. FTIR spectrum in the OH stretching region after activation of Cu-SAPO STA-7 at 573 K in O_2.

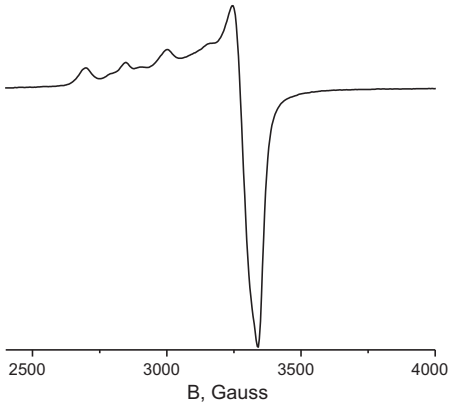

Fig. 11. ESR spectrum of Cu SAPO STA-7 calcined, dehydrated, activated in O_2 at 573 K and evacuated.

ZSM-5(IE) shows high conversion (approaching 80%) at 643–723 K, Cu-SAPO STA-7(DS) shows low activity (<20% conversion) and Cu-SAPO STA-7(IE) shows no activity. This difference is likely to arise from the difference in pore size between the ZSM-5 structure (5–5.5 Å) and the small pore STA-7 structure (4 Å) which hinders access of propene to active sites. The difference in performance between the Cu-SAPO STA-7 samples prepared by direct synthesis and aqueous ion exchange, both of which are crystalline to powder X-ray diffraction, is likely to arise from the differences in the distributions of Cu^{2+} (Table 3). Although bulk copper content, as determined by elemental analysis, is similar, XPS reveals that there is considerable surface copper enrichment in the ion exchanged SAPO (an effect not seen for the zeolite). This is confirmed by electron microscopic studies (Supplementary Data). The SAPO STA-7 framework is not stable enough to resist the strong incident beam (200 kV), so no lattice fringes are observable. The TEM images of calcined Cu SAPO STA-7(DS) and Cu-SAPO STA-7(IE) materials, in which the average Cu particle size is larger than 50 Å, do not indicate the state of Cu prior to contact with the electron beam. However, these data clearly show that the particles are well-dispersed over the Cu-SAPO STA-7(DS) crystals, but those in Cu-SAPO STA-7(IE) are mainly located on its outer surface. The exchange of

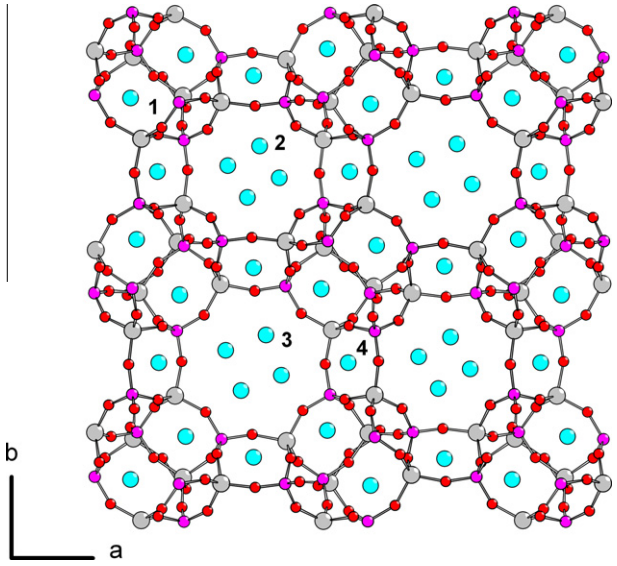

Fig. 12. Structure of calcined Cu SAPO STA-7, viewed down the c axis and showing all symmetry related positions of Cu^{2+} cations (blue spheres). Examples of the four different sites located are labelled (Cu1 as 1, Cu2 as 2, Cu3 as 3 and Cu4 as 4). Note that only a small fraction of these sites is occupied.

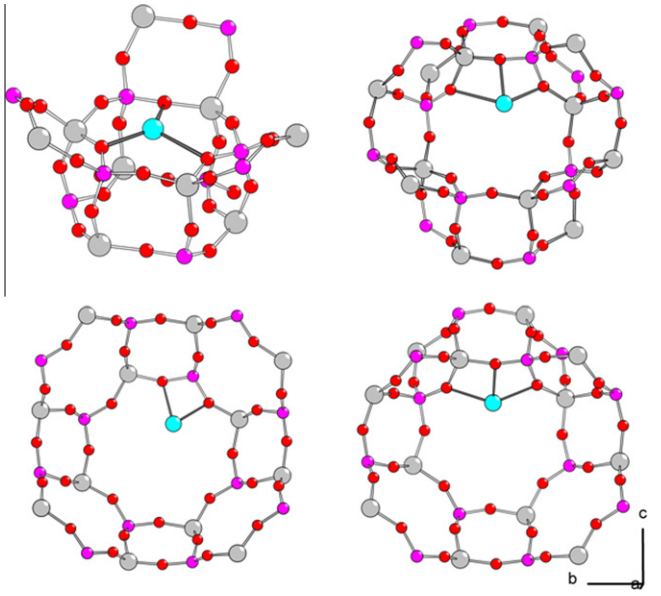

Fig. 13. Plots showing the local environments of sites (above left) Cu1, (above right) Cu2, (below left) Cu3 and (below right) Cu4.

Table 3
Properties of copper-containing catalysts investigated for NO SCR.

Catalyst	Si/(Si + Al + P) ratio[a]	Cu content[a], wt.%	Cu/M[b]		Crystal shape and size[d], μm	BET[e] $m^2 g^{-1}$
			Bulk[a]	Surface[c]		
Cu-ZSM-5(IE)	14[f]	2.9	0.49	0.23 (0.36)	Rods, 0.5 × 2	400
Cu-SAPO STA-7(IE)	0.135	3.3	0.25	1.98 (0.70)	Tetragonal prisms, 2–3	350
Cu-SAPO STA-7(DS)	0.125	4.2	0.33	0.12 (0.11)	Cuboids, 1–2	550

[a] Determined by elemental analysis.
[b] M is Si and Al when SAPO materials and zeolites, respectively.
[c] Determined by XPS. The values given in parentheses are the Cu/M ratios of the corresponding samples after calcination in air at 823 K for 4 h.
[d] Determined by SEM.
[e] Calculated from N_2 adsorption data.
[f] Si/Al ratio.

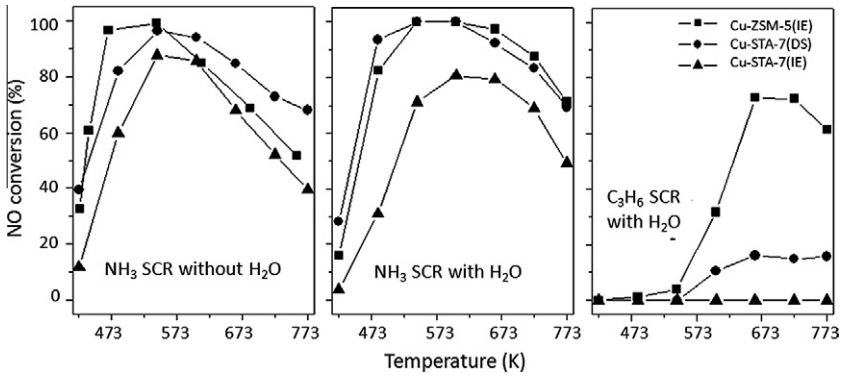

Fig. 14. Catalytic conversions of NO as a function of temperature over Cu-ZSM-5(IE) (■), Cu-SAPO STA-7(DS) prepared by direct synthesis and calcination (●) and Cu-SAPO STA-7(IE) prepared by ion exchange of calcined SAPO STA-7 (▲). The reaction composition was 500 ppm NO, 500 ppm NH_3 or 2000 ppm C_3H_6, and 5% O_2 with or without 10% H_2O in N_2 and with a total flow rate of 3300 cm^3 min^{-1} (100,000 h^{-1} GHSV).

Cu^{2+} cations to SAPO STA-7 may be limited to regions close to the surface, because the diameter (6.0 Å) of their hydrated form [54] is rather large to diffuse through the different types of 8-ring windows (3.8 × 3.8 and 3.9 × 3.9 Å) in SAV-type materials without loss of water ligands. Given the role of copper-cyclam complex as an SDA in Cu SAPO STA-7, by contrast, the Cu species in its calcined form could be dispersed in a highly homogeneous manner throughout the crystals.

4. Conclusions

A new preparative route to a copper-containing SAPO (with the SAV topology) has been established that involves the use of copper cyclam as a structure directing agent. Upon calcination in flowing oxygen, microporous Cu,H-SAPO STA-7 (also written Cu-SAPO STA-7) is produced, which is a highly active catalyst for the selective catalytic reduction of NO with NH_3.

The hydrothermal synthetic route uses copper cyclam complex, together with tetraethylammonium ions as co-templates for crystallisation of SAPO STA-7. A combination of UV–visible and ESR spectroscopies and chemical analyses indicate that the complex is retained intact within the structure. Despite the presence of paramagnetic Cu^{2+}, MAS NMR spectra of the as-prepared solid are readily obtained, and indicate that all Si is present substituting in P positions in the framework. Single crystal diffraction from crystals 60 μm in all dimensions confirms the location of the complex and the TEA^+ cations as co-SDAs within the larger and smaller cages of STA-7, respectively. Combining all analytical data gives an idealised charge balanced unit cell composition $[Cu(cyclam)]_2[TEA]_2Al_{24}Si_6P_{18}O_{96}\cdot 11H_2O$ where each large cavity is occupied by a copper cyclam complex and each smaller cage by a TEA^+ cation. Analysis suggests that the actual copper content is typically a little lower, e.g. $[Cu(cyclam)]_{1.8}[TEA]_2Al_{24}Si_{5.6}P_{18.4}O_{96}\cdot 11H_2O$. It is also possible to prepare Cu SAPO STA-7 with small particle size, suitable for catalysis, by seeding the same preparation.

Calcination of the as-prepared solid in oxygen removes the organic molecules included during synthesis, leaving extra framework Cu^{2+} cations distributed evenly throughout the pore space. IR spectroscopy indicates the presence of bridging hydroxyl groups: $Cu_{1.8}H_2Al_{24}Si_{5.6}P_{18.4}O_{96}$ and, via the use of NO as a probe molecule, suggests the presence of at least four different environments for the Cu^{2+} cations. Rietveld analysis of synchrotron X-ray powder diffraction data of the calcined material locates four positions for the Cu^{2+} cations. The most occupied site is within a 6MR that opens into the larger cage of STA-7, but there are also sites where the Cu^{2+} cation is within the 8MR windows that separate large cages (Cu2), small cages (Cu3) and large and small cages (Cu4). Cu1, the most highly occupied site, is similar to the only site determined for Cu^{2+} in the structurally-related Cu-chabazite zeolite Cu SSZ-13 (which is known to be active in the SCR of NO with NH_3). Variable temperature diffraction suggests there is an increase in the occupancy of the Cu1 site as the temperature is raised from 293 to 673 K.

Cu-SAPO STA-7 with particle size 2 μm (prepared by calcining directly synthesised copper-containing material) is a very good catalyst for the SCR of NO with NH_3, in the absence or presence of water vapour. Its performance is comparable with that of Cu-ZSM-5 prepared by ion exchange and exceeds that of a sample of Cu-SAPO STA-7 of similar copper content prepared by aqueous ion exchange of calcined SAPO STA-7. XPS and TEM analyses indicate that a more homogeneous distribution of Cu is achieved via direct synthesis.

We are currently extending the method of direct synthesis of Cu^{2+}-containing SAPOs to materials of different framework topologies, with the aim of developing a general route to catalysts with homogeneous metal cation distributions, the preparation of which does not require an aqueous ion exchange step that can result in hydrolytic damage of the aluminophosphate-based framework.

Acknowledgements

We gratefully acknowledge the following for financial support: The University of St. Andrews; the EC STREP program 'DeSANNS' (SES6-CT-2005-020133); EPSRC grant EP/EO41825/1 (SEA). The work at POSTECH was supported by the National Research Foundation of Korea (NRF) grant (No. 20100028712) funded by the Korea government (MEST). We thank Professor John C. Walton (St. Andrews) for help in performing the ESR experiments, Professor Chiu C. Tang for assistance at the I11 beamline at the Diamond Light Source (DLS) and DLS for beamtime.

Appendix A. Supplementary data

Supplementary data associated with this article can be found, in the online version, at doi:10.1016/j.micromeso.2011.04.039.

References

[1] P. Forzatti, L. Lietti, Heter. Chem. Rev. 3 (1996) 33.
[2] S. Brandenberger, O. Kröcher, A. Tissler, R. Althoff, Catal. Rev. Sci. Eng. 50 (2008) 492.
[3] M. Iwamoto, H. Furukawa, Y. Mine, F. Uemura, S.I. Mikuriya, S. Kagawa, J. Chem. Soc. Chem. Commun. (1986) 1272.
[4] M. Iwamoto, Catal. Today 10 (1991) 57.
[5] M. Iwamoto, H. Yahiro, N. Mizuno, W.X. Zhang, Y. Mine, H. Furukawa, S. Kagawa, J. Phys. Chem. 96 (1992) 9360.
[6] D.J. Liu, H.J. Robota, Catal. Lett. 21 (1993) 291.
[7] B. Modén, P. Da Costa, B. Fonfé, D.K. Lee, E. Iglesia, J. Catal. 209 (2002) 75.
[8] M.H. Groothaert, J.A. van Bokhoven, A.A. Battiston, B.M. Weckhuysen, R.A. Schoonhetdt, J. Am. Chem. Soc. 125 (2003) 7629.
[9] H. Sjovall, L. Olsson, E. Fridell, R.J. Blint, Appl. Catal. B: Environ. 64 (2006) 180.
[10] M.Y. Kustova, S.B. Rasmussen, A.L. Kustov, C.H. Christensen, Appl. Catal. B Environ. 67 (2006) 60.
[11] I. Melian-Cabrera, S. Espinosa, J.C. Groen, B. Van de Linden, F. Kapteijn, J.A. Moulijn, J. Catal. 238 (2006) 250.
[12] D.W. Fickel, E. D'addio, J.A. Lauterbach, R.F. Lobo, Appl. Catal. B Environ. 102 (2011) 441.
[13] S. Kieger, G. Delahay, B. Coq, B. Neveu, J. Catal. 183 (1999) 267.
[14] M. Iwamoto, H. Yahiro, K. Tanda, N. Mizuno, Y. Mine, S. Kagawa, J. Phys. Chem. 95 (1991) 3727.
[15] T. Komatsu, M. Nunokawa, I.S. Moon, T. Takahara, S. Namba, T. Yashima, J. Catal. 148 (1994) 427.
[16] P.J. Anderson, J.E. Bailie, J.L. Casci, H.Y. Chen, J.M. Fedeyko, R.K.S. Foo, R.R. Rajaram WO/2008/132452 A2, 2008.
[17] I. Bull, R.S. Boorse, W.M. Jaglowski, G.S. Koermer, A. Moini, J.A. Patchett, X.M. Xue, P. Burk, J.C. Dettling, M.T. Caudle, US Patent 0226,545, 2008.
[18] S.I. Zones, US Patent 4544,538, 1985.
[19] S.I. Zones, US Patent 5194,235, 1993.
[20] D.W. Fickel, R.F. Lobo, J. Phys. Chem. C 114 (2010) 1633.
[21] S.T. Korhonen, D.W. Fickel, R.F. Lobo, B.M. Weykhuysen, A.M. Beale, Chem. Commun. 47 (2011) 800.
[22] T. Ishihara, M. Kagawa, F. Hadama, Y. Takita, J. Catal. 169 (1997) 93.
[23] I. Bull, G.S. Koermer, A. Moini, S. Unverricht, US Patent 0196,812 A1, 2009.
[24] P.A. Wright, M.J. Maple, A.M.Z. Slawin, V. Patinec, R.A. Aitken, S. Welsh, P.A. Cox, J. Chem. Soc. Dalton Trans. 8 (2000) 1243.
[25] M. Castro, R. Garcia, S.J. Warrender, P.A. Wright, P.A. Cox, A. Fecant, C. Mellot-Draznieks, N. Bats, Chem. Commun. (2007) 3470.
[26] I. Deroche, L. Gaberova, G. Maurin, M. Castro, P.A. Wright, P.L. Llewellyn, J. Phys. Chem. C 112 (2008) 5048.
[27] P. Cubillas, M. Castro, K.E. Jelfs, A.J.W. Lobo, B. Slater, D.W. Lewis, P.A. Wright, S.M. Stevens, M.W. Anderson, Cryst. Growth Des. 9 (2009) 4041.
[28] M. Castro, S.J. Warrender, P.A. Wright, D. Apperley, Y. Belmabkhout, G. Pirnberger, H.-K. Min, M.B. Park, S.B. Hong, J. Phys. Chem. C 113 (2009) 15731.
[29] D. Tzoulaki, L. Heinke, M. Castro, P. Cubillas, M.W. Anderson, W. Zhou, P.A. Wright, J. Kärger, J. Am. Chem. Soc. 132 (2010) 11665.
[30] N. Rajic, A. Meden, P. Sarv, V. Kaucic, Micropor. Mesopor. Mater. 24 (1998) 83.
[31] R. Garcia, I.J. Shannon, A.M.Z. Slawin, W. Zhou, P.A. Cox, P.A. Wright, Micropor. Mesopor. Mater. 58 (2003) 91.
[32] R. Garcia, T.D. Coombs, I.J. Shannon, P.A. Wright, P.A. Cox, Top. Catal. 24 (2003) 115.
[33] R. Garcia, E.F. Philp, A.M.Z. Slawin, P.A. Wright, P.A. Cox, J. Mater. Chem. 11 (2001) 1421.
[34] P.S. Wheatley, R.E. Morris, J. Solid State Chem. 167 (2002) 267.
[35] F.Z. Duan, J.Y. Li, W. Sun, P. Chen, J.H. Yu, R.R. Xu, Sci. China – Chem. 53 (2010) 2159–2163.
[36] A.R. Balkenende, C.J.G. Vandergrift, E.A. Meulenkamp, J.W. Geus, Appl. Surf. Sci. 68 (1993) 161.
[37] C. Lamberti, S. Bordiga, A. Zecchina, M. Salvalagio, F. Geobaldo, C. Otero Arean, J. Chem. Soc. Faraday Trans. 94 (1998) 1519.
[38] G. Turnes Palomino, S. Bordiga, A. Zecchina, G.L. Marra, C. Lamberti, J. Phys. Chem. B 104 (2000) 8641.
[39] A. Frache, M. Cadoni, C. Bisio, L. Marchese, A.J.S. Mascarenhas, H.O. Pastore, Langmuir 18 (2002) 6875.
[40] K. Hadjiivanov, H. Knözinger, Phys. Chem. Chem. Phys. 3 (2009) 1132.
[41] G.M. Sheldrick, Acta Crystallogr. A 64 (2008) 112.

[42] S.P. Thompson, J.E. Parker, J. Potter, T.P. Hill, A. Birt, T.M. Cobb, F. Yuan, C.C. Tang, Rev. Sci. Instrum. 80 (2009) 075107–075109.
[43] A.C. Larson, R.B. Von Dreele, General Structure Analysis System (GSAS), Los Alamos National Laboratory, USA, 1994.
[44] Y. Dong, G.A. Lawrance, L.F. Lindoy, P. Turner, J. Chem. Soc. Dalton Trans. (2003) 1567.
[45] S.V. Rosokha, Y.D. Lampeka, I.M. Maloshtan, J. Chem. Soc. Dalton Trans. (1993) 1264.
[46] K.J.D. Mackenzie, M.E. Smith, Multinuclear Solid-State NMR of Inorganic Materials, Pergamon Press, 2002.
[47] R.Y. Pei, Z.J. Tian, Y. Wei, K.D. Li, Y.P. Xu, L. Wang, H.J. Ma, Mater. Lett. 64 (2010) 2118.
[48] F.A. Cotton, G. Wilkinson, C.A. Murillo, M. Bochmann, Advanced Inorganic Chemistry, sixth ed., John Wiley and Sons, 1999.
[49] K. Hadjiivanov, J. Saussey, J.L. Freysz, J.-C. Lavalley, Catal. Lett. 52 (1998) 103.
[50] M. Mihaylov, A. Penkova, K. Hadjiivanov, M. Daturi, J. Mol. Catal. A Chem. 249 (2006) 40.
[51] J. Dedecek, Z. Sobalik, Z. Tvaruzkova, D. Kaucky, B. Wichterlova, J. Phys. Chem. 99 (1995) 16327.
[52] S.A. Yashnik, Z.R. Ismagilov, V.F. Anufrienko, Catal. Today 110 (2005) 310.
[53] B.F. Mentzen, G. Bergeret, J. Phys. Chem. C 111 (2007) 12512.
[54] L. Kielland, J. Am. Chem. Soc. 59 (1937) 1675.